Acoust. Sci. & Tech. **43**, 6 (2022)

TECHNICAL REPORT

Development of an ultrasonic complex vibration source that produces an elliptical vibration locus

Yoshihiro Miyata, Takuya Asami and Hikaru Miura*

Department of Electrical Engineering, College of Science and Technology, Nihon University, 1–8–14, Kanda-Surugadai, Chiyoda-ku, Tokyo, 101–8308 Japan

(*Received 1 April 2022, Accepted for publication 29 July 2022*)

Abstract: Conventional ultrasonic welding uses linear vibrations, but welding using an elliptical locus improves welding strength. Therefore, we developed a vibration source that generates an elliptical locus using a single longitudinal vibration transducer. Although vibration sources with an elliptical locus have been reported previously, they were designed using the equivalent transmission line method. In this paper, we used the finite element method to elliptical vibration source design, and we fabricated a vibration source and measured its characteristics. Bringing the resonance frequencies of the longitudinal and torsional vibration closer together allowed vibration with an elliptical locus to be obtained at a single frequency.

Keywords: Elliptical vibration locus, Complex vibration, Finite element method, Ultrasonic welding

1. INTRODUCTION

There have been many studies on ultrasonic welding of metals [1–5]. Since ultrasonic welding does not use heat, it can be used to join dissimilar metals with different melting points. Conventional ultrasonic welding uses a linear vibration displacement locus in only one direction on the welded object. Consequently, the welding area is small, the welding strength is low when the object is pulled in the direction of vibration due to the directionality of the joint trace, and the joining time is long due to the low vibration energy. In addition, because the vibration displacement is only in one direction, the rapid change in the stress direction during the reciprocating vibration causes a decrease in the welding strength [6].

To solve these problems, ultrasonic welding using two-dimensional vibration displacements that form a planar locus or an elliptical locus has been investigated [7–11]. This type of welding is superior to that using linear vibration displacement because there is less directionality in the vibration, so there is no directionality in the tensile strength, and this method can result in the superior welding strength.

Miura *et al.* investigated welding using a dumbbell vibration source with longitudinal and torsional vibrators that generate two-dimensional planar vibration displacements [12–14].

In addition, Miura *et al.* developed a dumbbell vibration source that used two longitudinal transducers rather than a torsional transducer [15].

Tsujino *et al.* developed vibration sources that generated vibration displacements with circular or elliptical trajectories [16–20]. Their results also demonstrated the superiority of circular or elliptical vibration displacement over linear vibration displacement. The equivalent transmission line method was used in the design of these vibration sources.

Muhammad *et al.* also investigated generating complex vibration by diagonally slitting a step-horn transmission rod [21]. They used a neural network and the finite element method (FEM) to develop a vibration source.

A helical slit can be used to generate a planar vibration at the tip of a transmission rod using a single longitudinal transducer. Harkness *et al.* investigated the suppression of electrical anti-resonance in torsional vibration using a helical slit, although they did not examine elliptical vibration displacement [22–24].

The helical slit generates longitudinal and torsional vibrations simultaneously by using the contraction of longitudinal and torsional vibrational resonances, and that the two resonance frequencies are used to generate planar vibrational displacements [25].

Therefore, we developed a vibration source that uses a single longitudinal transducer to generate elliptical vibrations at a single frequency, thereby increasing the versatility of the design [26].

In this paper, we used the FEM to design a vibration

*e-mail: miura.hikaru@nihon-u.ac.jp
[doi:10.1250/ast.43.327]

source to generate an elliptical displacement locus at the tip of a transmission rod with helical slits using a single frequency.

2. ULTRASONIC COMPLEX VIBRATION SOURCE

Figure 1 provides an overview of our ultrasonic complex vibration source. The vibration source consisted of a 39 kHz bolt-clamped Langevin transducer (HEC-3039P4B, Honda Electronics), a flange-integrated exponential horn (A2017; thick end face diameter, 30 mm; thin end face diameter, 12 mm; amplitude amplification ratio, 3), and transmission rod (SUS303; diameter, 12 mm; length, L) (Fig. 1(a)). The length in the direction of the central axis was set to 0 mm at the left end of the transducer. Figure 1(b) shows the cross section 4 mm from the tip. The side of the transmission rod contained helical slits with a semicircular cross-section, and the depth radius was R, the number of rotations was one, and the number of slits was two.

Because this vibration source is intended to be used for welding, we focused on the vibration at the tip of the transmission rod. We refer to the vibration in the direction of the central axis of the tip as longitudinal vibration and that in the circumferential direction as torsional vibration. First, to understand the characteristics of the ultrasonic longitudinal transducer, the admittance was measured by using an impedance analyzer (ZGA5920, NF) with the driving voltage of the ultrasonic longitudinal transducer constant at 1.0 V (effective value). The resonance frequency of the longitudinal vibration was 39.5 kHz and the admittance was 154 mS. Because the resonance frequency of the resonator alone was 39.5 kHz, the resonance frequency of the longitudinal vibration of the entire vibration source using an exponential horn and a transmission rod without a slit needed to be 39.5 kHz. A simulation analysis calculated that transmission rod length L needed to be about 60 mm.

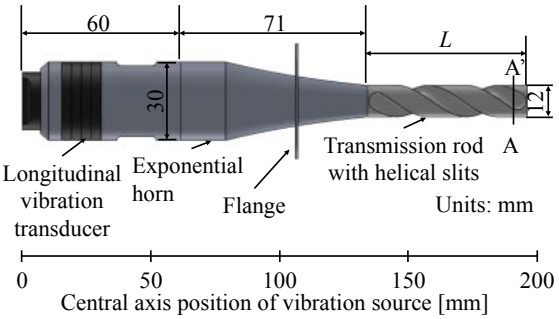

(a) Schematic of the entire ultrasonic complex vibration source.

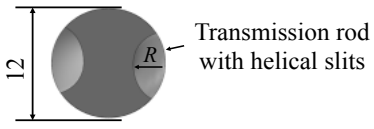

(b) Cross-sectional view of transmission rod in the A-A' plane.

Fig. 1 Schematic of the ultrasonic complex vibration source.

3. DESIGN OF ULTRASONIC VIBRATION SOURCE

To generate elliptical vibration displacement at the tip of a transmission rod using a single frequency, it is necessary to minimize the difference between the resonance frequencies of longitudinal and torsional vibration. We investigated how to bring the two resonance frequencies closer together by varying the transmission rod length and the helical slit depth. The two resonance frequencies are f_1 for the lower value and f_{f2} for the higher value. Piezoelectric analysis was performed using COMSOL Multiphysics, which is analysis software that uses the FEM. The material constants of the metallic materials used in the analysis are shown in Table 1. In addition, irons are used for the coupling screws. The piezoelectric material is PZT4, and the material constants are shown in Table 2.

3.1. Transmission Rod Length and Helical Slit Depth

The flange used to fix the ultrasonic complex vibration source may affect the generation of torsional resonance; thus, this section discusses the vibration source with the flange removed from the vibration source shown in Fig. 1.

To generate elliptical vibration displacement, the difference in resonance frequency between longitudinal and torsional vibrations must be reduced. Therefore, simulation analysis was conducted in which the transmission rod length, L, and the helical slit depth, R, were varied. The analysis was performed for L of 58–62 mm and R of 3.0–4.0 mm.

Figure 2 shows the analysis results with L on the horizontal axis and R on the vertical axis, and the difference in the resonance frequencies of the vertical and torsional vibrations as a contour plot. When L was constant, the frequency difference was minimum when R was 3.4 mm. The frequency difference did not change with

Table 1 Material constants of metallic materials.

Material name	Young's modulus [GPa]	Poisson's ratio	Density [kg/m^3]
A2017	73	0.33	2790
SUS303	197	0.3	7920
Iron	200	0.29	7870

Table 2 Material constants of piezoelectric materials.

Moduli	Unit	
Density	kg/m^3	7,500
c_{11}^{E}	GPa	139
c_{12}^{E}	GPa	78
c_{13}^{E}	GPa	74
c_{22}^{E}	GPa	139
c_{23}^{E}	GPa	74
c_{33}^{E}	GPa	115
c_{44}^{E}	GPa	26
c_{55}^{E}	GPa	26
c_{66}^{E}	GPa	31
e_{31}	Cm^{-2}	−5.2
e_{32}	Cm^{-2}	−5.2
e_{33}	Cm^{-2}	15.1
e_{24}	Cm^{-2}	12.7
e_{15}	Cm^{-2}	12.7
$\varepsilon_{11}^{S}/\varepsilon^{a0}$	—	763
$\varepsilon_{22}^{S}/\varepsilon^{a0}$	—	763
$\varepsilon_{33}^{S}/\varepsilon^{a0}$	—	663

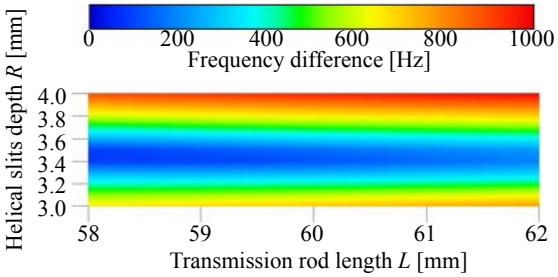

Fig. 2 Calculated difference in resonance frequency between the longitudinal and torsional vibrations.

L significantly within the range examined, but did increase somewhat with increasing length.

To generate elliptical vibration displacement at a single frequency, the frequency difference between resonance frequencies f_1 and f_2 must be small. Therefore, the range where the frequency difference was small was slit depths of 3.3–3.6 mm and transmission rod lengths of 58–62 mm. In addition, it is important to know the ratio of the vibration displacement at resonance for the longitudinal and torsional vibrations and the coupling of the vibration modes. Therefore, the vibration displacement ratio was obtained from the amplitude ratio of the displacement shown in Eq. (1) at the resonance frequency of both vibrations at the tip of the transmission rod.

$$\text{Amplitude ratio} = \left| \frac{\text{Displacement amplitude of torsional vibration}}{\text{Displacement amplitude of longitudinal vibration}} \right| \quad (1)$$

Figures 3(a) and 3(b) show the results for the displacement amplitude ratios at f_1 and f_2, respectively, in the same

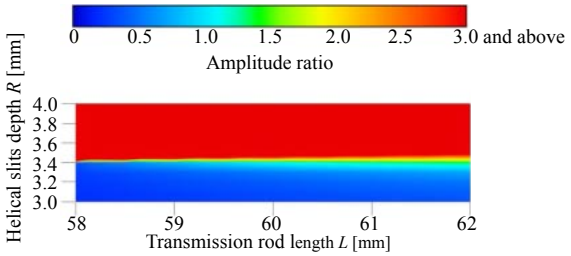

(a) Displacement amplitude ratio at resonance frequency f_1.

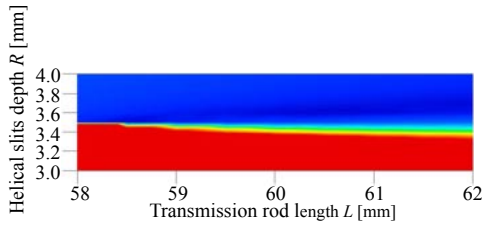

(b) Displacement amplitude ratio at resonance frequency f_2.

Fig. 3 Calculated displacement amplitude ratio. The displacement amplitude ratio is the torsional vibration displacement amplitude/longitudinal vibration displacement amplitude.

range and with the same axes as in Fig. 2. The displacement amplitude ratios are shown as contour plots on the same scale.

The displacement amplitude ratio at f_1 and f_2 should be 1.0–2.0 because a previous study showed that the vibration displacement with an elliptical shape was obtained even when the displacement amplitude ratio was about 1.6. Thus, the amplitude ratios at f_1 and f_2 were 1.0–2.0 for a slit depth of 3.4 mm and a transmission rod length of 60–62 mm. The helical slit depth and the transmission rod length were set to 3.4 and 61 mm, respectively, considering the frequency difference and the amplitude ratio, as well as the margin for dimensional error in the fabrication.

3.2. Vibration Distribution of an Ultrasonic Complex Vibration Source

We examined the vibration displacement distribution of the ultrasonic complex vibration source with the dimensions determined by the results so far (Fig. 4). The analytical model is shown in Fig. 1 without the fixing flange. Figure 4(a) shows the results of the analysis of the vibration displacement distribution at the resonance frequency f_1 (36.28 kHz). The horizontal axis is the position of the ultrasonic complex vibration source in the direction of the central axis and the vertical axis is the amplitude of the vibration displacement normalized to the maximum value of the vibration displacement amplitude. The longitudinal, torsional, and flexural vibration displacement amplitudes are shown by the blue, red, and green lines, respectively. The longitudinal and flexural displacement

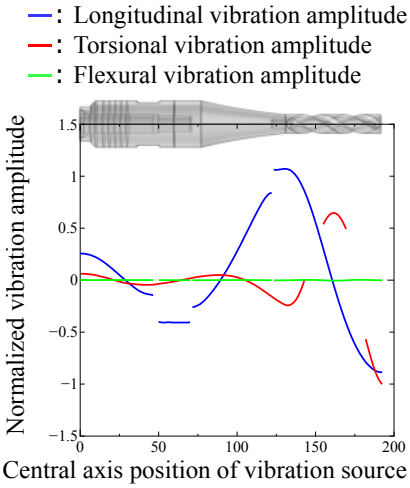

(a) Vibration displacement distribution at resonance frequency f_1.

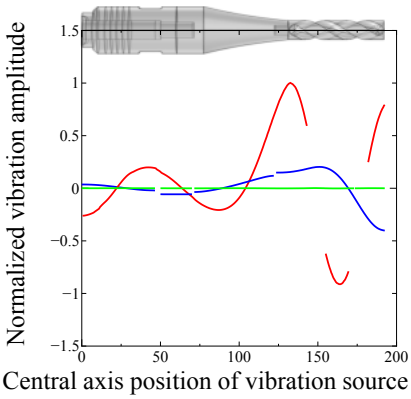

(b) Vibration displacement distribution at resonance frequency f_2.

Fig. 4 Calculated distributions of vibration displacements at two resonance frequencies.

amplitudes indicate the vibration displacement amplitude on the central axis of the vibration source. On the other hand, the displacement amplitude of torsional vibration was not on the central axis, so the vibration displacement amplitudes at the side of the vibration source, located 6 mm radially from the central axis, are shown. Some lines are discontinuous because there are no results for the surface cut away to form the helical slits and the void for the screw hole. The amplitude distribution of the longitudinal vibration was 1.5 wavelengths in total and that of the torsional vibration was 2.5 wavelengths in total. The longitudinal and torsional vibrations formed antinodes at the tip of the transmission rod with an amplitude ratio of 1.3. The flexural vibration was smaller than the longitudinal and torsional vibration.

Figure 4(b) shows the analysis results at f_2 (36.43 kHz). The distribution positions, the axes, and figure legends are the same as in Fig. 4(a). The amplitude distribution of the longitudinal vibration was 1.5 wavelengths in total and that of the torsional vibration was 2.5 wavelengths in total, as in Fig. 4(a). At the tip of the transmission rod, the longitudinal and torsional vibrations formed antinodes, and the amplitude ratio was 1.7. The flexural vibration was also smaller than the longitudinal and torsional vibration. These results showed that the elliptical vibration displacement could be obtained at the tip of the transmission rod for both resonance frequencies by considering the frequency difference and amplitude ratio.

3.3. Position of Fixing Flange

The flange for fixing the vibration source must have no effect on the vibration displacement distribution, even if the flange is fixed. The position of the flange, which had little effect on the vibration displacement at the longitudinal and torsional vibration resonance frequencies, was investigated by simulation analysis using the analytical model shown in Fig. 1. Because the resonance frequency of the torsional vibration is easily affected by the fixed flange, the analysis examined the locations where the presence or absence of the flange did not affect the vibration displacement. The position of the fixed flange was varied within the range including the nodes of the longitudinal vibration resonance and torsional vibration resonance distributed through the exponential horn.

The longitudinal vibration node was 90 mm from the edge of the resonator in the direction of the central axis (Fig. 4(a)) and the torsional vibration node was 104 mm from the edge of the resonator (Fig. 4(b)). In the analysis, the diameter of the flange was set to 44 mm and its thickness to 1 mm, and a fixed constraint was applied within 6 mm from the circumference of the flange to prevent the flange from vibrating.

Figure 5 shows the analysis results. The horizontal axis is the position of the flange where the vibration source is fixed and the vertical axis is the difference of the resonance

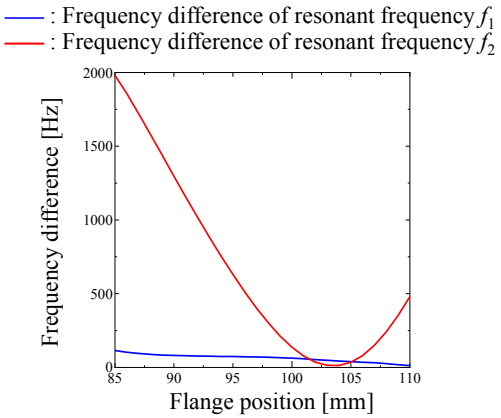

Fig. 5 Calculated flange installation position.

frequency. The blue line is the frequency difference from resonance frequency f_1 without the flange shown in Fig. 4(a), and the red line is the frequency difference from resonance frequency f_2 without the flange shown in Fig. 4(b). The frequency difference at f_2 decreased up to a flange position of 104 mm, and then increased again. This frequency difference reached a minimum of 13 Hz at 104 mm. In contrast, the frequency difference at f_1 was small in the range studied, but decreased as the flange position approached the transmission rod. The frequency difference was also small near the 104 mm position, at about 40 Hz.

Based on these results, the flange was located 104 mm from the edge of the resonator to minimize the effect on resonance frequencies f_1 and f_2. The position of the flange was close to the position of the torsional vibration nodes. The displacement amplitude ratio at the tip of the transmission rod at f_1 was about 1.4, and at f_2 it was about 1.5, which were important values.

The vibration displacement distribution of the vibration source when the position of the flange was 104 mm was analyzed. Figure 6(a) shows the results for the vibration displacement distribution at f_1 (36.3 kHz). The axes and parameters and the position of the vibration displacement distribution are the same as in Fig. 4. The longitudinal vibration was 1.5 wavelengths in total, and the torsional vibration was 2.5 wavelengths in total, as in Fig. 4(a). The longitudinal and torsional vibrations formed antinodes at the tip of the transmission rod. In addition, the flexural vibration was smaller than the longitudinal and torsional vibration. Compared with the results in Fig. 4(a), the flexural vibration was smaller, but the vibration distribution of the longitudinal, torsional, and flexural vibrations was the same.

Figure 6(b) shows the analysis results for the vibration displacement distribution at f_2 (36.4 kHz). The axes and parameters and the position of the vibration displacement distribution are the same as in Fig. 4(a). The longitudinal vibration was 1.5 wavelengths in total, and the torsional vibration was 2.5 wavelengths in total, as in Fig. 4(b). In addition, the longitudinal and torsional vibrations formed antinodes at the tip of the transmission rod. The flexural vibration was smaller than the longitudinal and torsional vibration. The vibration distribution of the longitudinal, torsional, and flexural vibration was the same as in Fig. 4(b).

These results suggest that a flange fixed close to the torsional vibration node had little effect on the vibration distribution and amplitude ratio, and that elliptical vibration displacement can be obtained at the tip of the transmission rod for use in practical applications, such as welding.

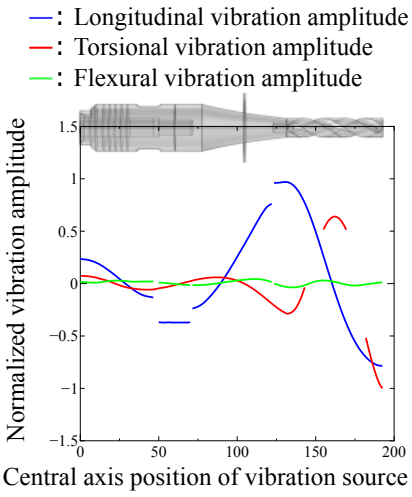

(a) Vibration displacement distribution at resonance frequency f_1.

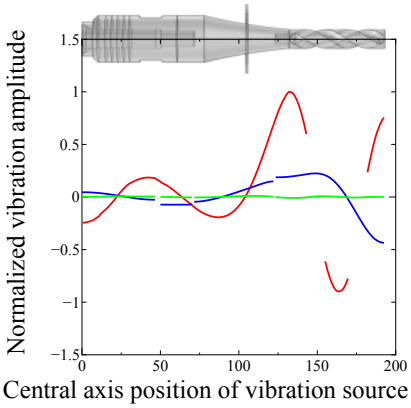

(b) Vibration displacement distribution at resonance frequency f_2.

Fig. 6 Calculated vibration displacement distribution with flange.

4. VIBRATION CHARACTERISTICS OF ULTRASONIC COMPLEX VIBRATION SOURCES

4.1. Frequency Response of the Vibration Source

An ultrasonic complex vibration source with the dimensions obtained from the analysis results shown in Sect. 3 was fabricated (Fig. 7). First, the frequency characteristics of the vibration source were measured by using an impedance analyzer (ZGA5920, NF) with a constant driving voltage of 1.0 V (effective value) for the vibration source. The frequency range was 36.0–37.5 kHz, and the measurements were performed in 1 Hz increments with the flange fixed.

Figure 8 shows the measurement results. The horizontal axis is the frequency and vertical axis is the conductance shown on a logarithmic scale. Two resonance frequencies were obtained in the measured range. The first resonance

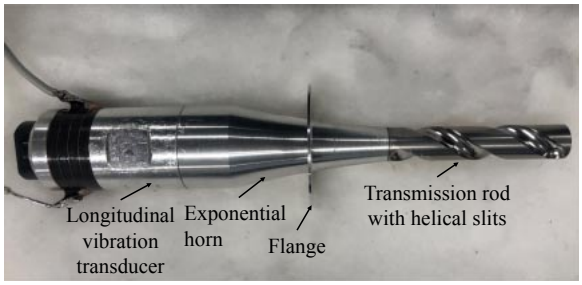

Fig. 7 Photograph of the fabricated ultrasonic complex vibration source.

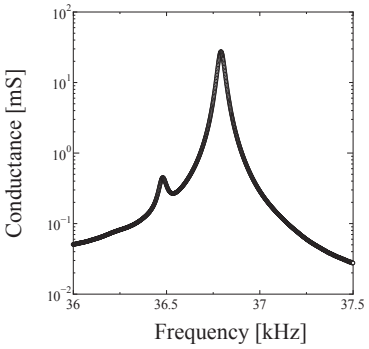

Fig. 8 Measured frequency response of the manufactured vibration source.

had a frequency of 36.5 kHz, with a conductance of 0.45 mS, and the second had a frequency of 36.8 kHz with a conductance of 27.2 mS.

4.2. Vibration Displacement Locus and Vibration Distribution of the Vibration Source

The vibration displacement amplitude at the tip of the transmission rod was measured to investigate the locus of the vibration displacement obtained by the vibration source. Two laser Doppler vibrometers were used to measure the vibration displacement: one to measure the longitudinal vibration displacement at the tip of the source, and the other to measure the torsional vibration displacement of the tip of the source at the lateral position (6 mm in the radial direction). The measurements were performed at the respective resonance frequencies with a constant input current of 50 mA to the vibration source.

Figure 9 shows the amplitude of the longitudinal displacement on the horizontal axis and the amplitude of the torsional displacement on the vertical axis, and the parameters are the two resonance frequencies. An elliptical vibration displacement locus (red line) was obtained at a frequency of 36.5 kHz, and the amplitude ratio of the longitudinal to torsional vibration was 1.3. A linear locus of vibration displacement (blue line) was obtained at a frequency of 36.8 kHz with an amplitude ratio of 1.1. These

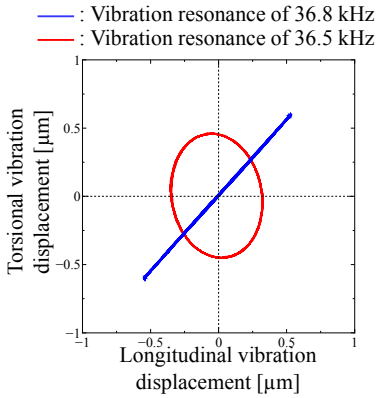

Fig. 9 Characteristics of the vibration locus.

results indicated that the measured amplitude ratios of both vibration displacements agreed with the analytical results.

Next, the displacement amplitudes of the longitudinal and torsional vibrations of the transmission rod were measured at both resonance frequencies where these vibration displacements were obtained. The displacement amplitude of the longitudinal vibration was measured using an annular electromagnetic vibration detector, which detects eddy currents in the plane perpendicular to the magnetic flux and the direction of vibration displacement by placing a coil close to transmission rod [27]. The output voltage of the detector is proportional to the vibration velocity. The displacement amplitude of the torsional vibration was measured by irradiation a small groove on the transmission rod with a laser Doppler vibrometer. The measurement conditions were the same as in Fig. 8, with a constant input current of 50 mA to the vibration source.

Figures 10(a) and 10(b) show the measured displacement amplitudes of the longitudinal and torsional vibrations of the transmission rod. The horizontal axes show the position of the vibration source in the direction of the central axis, and the vertical axes show the vibration displacement amplitude, normalized by the maximum value of each vibration displacement. The blue circles and red triangles indicate the measured longitudinal and torsional displacement amplitudes, respectively. The solid blue and red lines show the calculated amplitudes of the torsional and longitudinal vibration displacements, respectively. The red dotted lines are the vibration displacements of the torsional vibration that could not be measured due to the slit that were obtained by a separate analysis. The positions of the vibration sources for the longitudinal and torsional vibration analysis results are the same as those shown in Fig. 6.

Figure 10(a) shows the measured vibration displacement distribution at a frequency of 36.5 kHz and the calculated vibration displacement distribution at resonance frequency f_2. The measured longitudinal vibration distri-

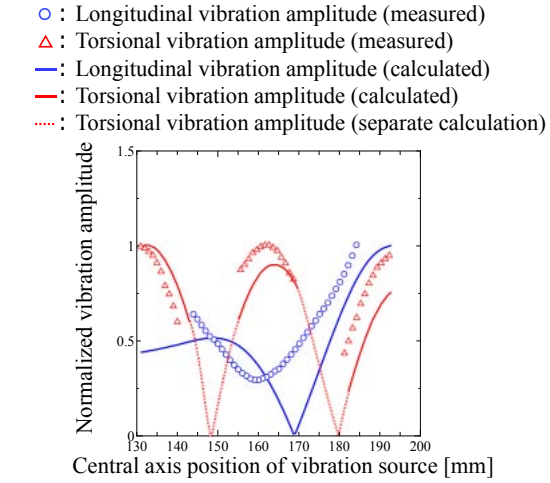

(a) Vibration displacement distribution at a frequency of 36.5 kHz.

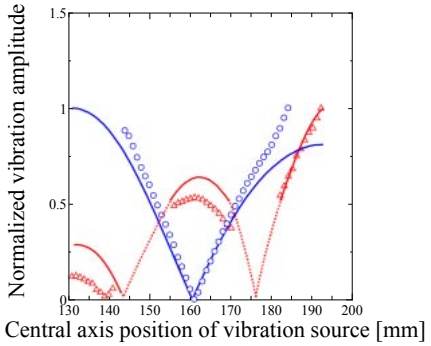

(b) Vibration displacement distribution at a frequency of 36.8 kHz.

Fig. 10 Relationship between the measured and calculated vibration displacement distribution.

bution had a node near 160 mm in the central axis direction, and the entire distribution was a half-wavelength vibration displacement distribution. However, the analyzed longitudinal vibration distribution had a node at 168 mm in the central axis direction, and the entire distribution was a half-wavelength vibration displacement distribution. Therefore, although there was a difference in the position of the nodes in the measured and calculated longitudinal vibration distributions, the vibration displacement distribution of the entire transmission rod was half a wavelength in measured and calculated cases, and was almost identical.

The measured torsional vibration distribution showed vibration displacement antinodes at central axis positions of 130, 165, and 190 mm, identical to the calculated values. The positions of the measured and calculated torsional vibration antinodes were similar, and the overall measured and calculated vibration displacement distribution was consistent at one wavelength.

Figure 10(b) shows the measured vibration distribution at a frequency of 36.8 kHz and the calculated vibration displacement distribution at f_1. The measured longitudinal vibration displacement distribution had a node at 160 mm in the central axis direction, and the entire distribution was a half-wavelength vibration displacement distribution, identical to the calculated values. Therefore, the nodes of measured and calculated longitudinal vibration distributions were similar, and the trend of the measured and calculated vibration displacement distribution was the same at half a wavelength.

The measured torsional vibration had vibration displacement antinodes at 130, 165, and 190 mm in the central axis direction, with the node near 140 mm, identical to the calculated values, suggesting that the overall measured and calculated vibration distribution was consistent at one wavelength.

These results showed that the vibration source measured resonance frequency of 36.5 kHz and calculated resonance frequency f_2 were the same vibration mode, and the vibration source measured resonance frequency of 36.8 kHz and calculated resonance frequency f_1 obtained by analysis were also the same vibration mode. The resonance frequencies of the two vibration modes could be brought closer together by obtaining the correct values for the transmission rod length and the helical slit depth of the vibration source, and that an elliptical vibration locus could be obtained at the tip of the transmission rod.

5. CONCLUSION

We developed an ultrasonic complex vibration source using a transmission rod with helical slits to obtain an elliptical vibration displacement at a single frequency. The design and vibration characteristics of the manufactured ultrasonic complex vibration source were investigated. The results were as follows.

(1) By setting the helical slit depth and the transmission rod length to appropriate values, the frequency difference between resonance frequencies f_1 and f_2 was reduced and the displacement of longitudinal and torsional vibrations formed antinodes at the tip of the transmission rod. The calculation results showed that the frequency difference between resonance frequencies f_1 and f_2 was reduced by setting appropriate values for the transmission rod and transmission rod length.

(2) The flange used to fix the vibration source must not affect the vibration mode even if the flange is fixed. Therefore, the flange position was examined to prevent it interfering with the resonance generation. Flanges could be fixed near the torsional vibration nodes with minimal effects on f_1 and f_2.

(3) The ultrasonic complex vibration source had resonance at frequencies of 36.5 and 36.8 kHz. An elliptical vibration displacement locus was obtained

at a driving frequency of 36.5 kHz, and a linear vibration displacement locus was obtained at a driving frequency of 36.8 kHz.

(4) The calculated distributions of the longitudinal and torsional vibration displacements at each resonance frequency agreed closely with the measured vibration displacement distributions.

Based on results, the design method considering the transmission rod length, the slit depth, and the flange position using the FEM brought the resonance frequencies of the two vibration modes closer together and the elliptical vibration displacement was obtained at a single frequency. Our method could be used for vibration sources with frequencies other than those studied here.

ACKNOWLEDGEMENTS

This work was supported by JSPS KAKENHI Grant No. 19K14863.

REFERENCES

[1] H. P. C. Daniels, "Ultrasonic welding," *Ultarasonics*, **3**, 190–196 (1965).

[2] J. Yang and B. Cao, "Investigation of resistance heat assisted ultrasonic welding of 6061 aluminum alloys to pure copper," *Mater. Des.*, **74**, 19–24 (2015).

[3] J. Tsujino, S. Ihara, Y. Harada, K. Kasahara and M. Shimizu, "Characteristics of coated copper wire specimens using high frequency ultrasonic complex vibration welding equipments," *Ultrasonics*, **42**, 121–124 (2004).

[4] E. A. Neppiras, "Ultrasonic welding of metals," *Ultrasonics*, **3**, 128–135 (1965).

[5] A. P. Hulst, "Macrosonics in industry 2. Ultrasonic welding of metals," *Ultrasonics*, **10**, 252–261 (1972).

[6] H. Ji, J. Wang and M. Li, "Evolution of the bulk microstructure in 1100 aluminum builds fabricated by ultrasonic metal welding," *J. Mater. Process. Technol.*, **214**, 175–182 (2014).

[7] J. Tsujino, T. Mori, T. Onozato and K. Hasegawa, "Welding characteristics of ultrasonic wire bonding using high-frequency vibration systems," *Jpn. J. Appl. Phys.*, **32**, 2435–2440 (1993).

[8] J. Tsujino, Y. Ishii, T. Shiraki and H. Ymazaki, "Ultrasonic plastic welding using 90 kHz upper and lower vibration systems," *Jpn. J. Appl. Phys.*, **33**, 3065–3070 (1994).

[9] J. Tsujino, T. Tamura, T. Uchida and T. Ueoka, "Characteristics of two-vibration-system ultrasonic plastic welding with 90 kHz and 20 kHz vibration systems at right angles," *Jpn. J. Appl. Phys.*, **35**, 5884–5889 (1996).

[10] J. Tsujino, M. Sakai, H. Ando, T. Negishi, Y. Murayama and H. Furuya, "Welding characteristics of ultrasonic wire bonding using the same or a different frequency complex vibration welding tips," *J. Appl. Phys.*, **28**, 137–139 (1988).

[11] J. Tsujino, H. Yoshihara, T. Itoh, K. Inujima and Y. Hirano, "Temperature rise and welding characteristics of ultrasonic wire bonding using 190 kHz linear, circular and square vibration loci and 600 kHz linear vibration locus welding tips," *Jpn. J. Appl. Phys.*, **37**, 3009–3012 (1998).

[12] T. Asami and H. Miura, "Longitudinal–torsional vibration source consisting of two transducers with different vibration modes," *Jpn. J. Appl. Phys.*, **55**, 07KE08, 1–5 (2016).

[13] T. Asami, Y. Tamada, Y. Higuchi and H. Miura, "Ultrasonic metal welding with a vibration source using longitudinal and torsional vibration transducers," *Jpn. J. Appl. Phys.*, **56**, 07JE02, 1–5 (2017).

[14] Y. Tamada, T. Asami and H. Miura, "Welding characteristics of Cu and Al plates using planar vibration by a dumbbell-shaped ultrasonic complex vibration source," *Jpn. J. Appl. Phys.*, **57**, 07LE12, 1–6 (2018).

[15] N. Saegusa, T. Asami and H. Miura, "Ultrasonic complex vibration source using two longitudinal vibration transducers and a uniform rod with diagonal slits," *Jpn. J. Appl. Phys.*, **60**, SDDD09, 1–7 (2021).

[16] J. Tsujino and T. Ueoka, "Ultrasonic seam welding system using a complex vibration circular disk in transverse and torsional vibrations," *Jpn. J. Appl. Phys.*, **38**, 3307–3311 (1999).

[17] A. Suzuki and J. Tsujino, "Load characteristics of ultrasonic motors with a longitudinal–torsional converter and various nonlinear springs for inducing static pressure," *Jpn. J. Appl. Phys.*, **41**, 3267–3271 (2002).

[18] A. Suzuki, M. Kihara, Y. Katumata and J. Tsujino, "Configuration of a transverse vibration rod type ultrasonic motor using three longitudinal transducers driven in three different vibration phases," *Jpn. J. Appl. Phys.*, **43**, 2901–2904 (2004).

[19] J. Tsujino, T. Mori, T. Onozato and K. Hasegawa, "Welding characteristics of ultrasonic wire bonding using high-frequency vibration systems," *Jpn. J. Appl. Phys.*, **32**, 2435–2440 (1993).

[20] J. Tsujino, K. Nakai, K. Sako, N. Ikegami, K. Noda and R. Suzuki, "Load characteristics and vibration loci at the driving surfaces of ultrasonic rotary motor using a longitudinal–torsional vibration converter," *Jpn. J. Appl. Phys.*, **37**, 2960–2965 (1998).

[21] M. B. Shahid, J. Jung and D. Park, "Finite element analysis coupled artificial neural network approach to design the longitudinal–torsional mode ultrasonic welding horn," *Int. J. Adv. Manuf. Technol.*, **107**, 2731–2743 (2020).

[22] P. Harkness, A. Cardoni and M. Lucas, "Ultrasonic rock drilling devices using longitudinal–torsional compound vibrations," *2009 IEEE Int. Ultrasonics Symp. Proc.*, pp. 2088–2091 (2009).

[23] H. Al-Budairi, M. Lucas and P. Harkness, "A design approach for longitudinal–torsional ultrasonic transducers," *Sens. Actuators A*, **198**, 99–106 (2013).

[24] A. Cardonia, P. Harkness and M. Lucasa, "Ultrasonic rock sampling using longitudinal–torsional vibrations," *Phys. Proc.*, **3**, 125–134 (2010).

[25] S. Oishi, Y. Miyata, T. Asami and H. Miura, "Welding characteristics of coated twisted wire and copper plate by ultrasonic vibration source using a transmission rod with helical slits," *Jpn. J. Appl. Phys.*, **59**, SKKD11, 1–10 (2020).

[26] Y. Miyata, T. Asami and H. Miura, "Vibration characteristics of ultrasonic complex vibration source using transmission rod with different cross-sectional area," *Proc. 42th Symp. Ultrasonic Electronics*, 2Pb4-5 (2021).

[27] J. Tsujino, "Studies on the ring type magnetic ultrasonic vibration detector," *Jpn. J. Appl. Phys.*, **23**, Suppl. 23-1, 212–214 (1982).